

A lattice Boltzmann-Based Study of Plasma Sprayed Particles Behaviours

R. Djebali¹, B. Pateyron² and M. ElGanaoui³

Abstract: Axisymmetric lattice Boltzmann (LB) model is developed to investigate the interaction of momentum and heat between plasma hot gas and Alumina powders. The plasma flow is simulated using a double population lattice Boltzmann model and the plasma-particles interaction is modeled based on a Lagrangian approach for the motion and heat transfer equations. The present results show that the LB method is an efficient and powerful tool to comprehend and explain the very high complexity of the plasma jet physics as well as it preserves effectively the computational cost. The present results for the centerline temperature and velocity profiles agree well with the previous experimental and various numerical approaches findings. Furthermore, our results for the plasma-particles interactions are in good agreement with the Finite-Differences results of the *Jets&Poudres* code for particles motion and heat-up.

Keywords: Lattice Boltzmann method, plasma jet, plasma spraying, in-flight-particles behaviours.

1 Introduction

The plasma spraying processes play an important role in technological surface treatment; they are also sources of experimental and numerical works to achieve high performance. This process has currently many particular features which attract special attention [Arcondéguy, Gasgnier, Montavon, Pateyron, Denoirjean, Grimaud and Huguet (2007); Ben Ettouil, Mazhorova, Pateyron, Ageorges, El Ganaoui and Fauchais (2008); Xie, Koshizuka and Oka (2007); Brillhac, Pateyron, Delluc, Coudert and Fauchais (1995); Siagam, Brenner, Giese and Wesling (2008); Chen, Heberlein, Pfender, Pateyron, Delluc, Elchinger and Fauchais (1995); Del-

¹ Preparatory Inst. of Eng. School, Mrezka, Nabeul 8000, Tunisia. jbelii_r@hotmail.fr, ridha.djebali@ipein.rnu.tn

² CNRS-SPCTS / CEC 12, Rue Atlantis 87068, Limoges, France.

³ LERMAB, Inst. Carnot, Univ. Henri Poincaré, Nancy, France.

luc, Ageorges, Pateyron and Fauchais (2005); Dilawari and Szekely (1987); Ghelichi, Bagherifard, Pariente, Guagliano and Vezzù (2010)]. Such a process offers a wide range of test cases for numerical analysts in spite of the high complexity due to coupled heat and mass transport properties and high thermal gradients and that these characteristics are perfectly non-linear [Chen, Heberlein, Pfender, Pateyron, Delluc, Elchinger and Fauchais (1995)]. Temperature and velocity fields in the plasma jet affect the particles trajectories and their thermal histories and thus the quality of the obtained coating [Ben Ettouil, Mazhorova, Pateyron, Ageorges, El Ganaoui and Fauchais (1987); Pateyron (1987); Li, Saheli, Khaleel and Garmestani (2006); Siagam, Brenner, Giese and Wesling (2008)]. Available modeling works on plasma jets are almost all based on the assumption of steady flow in time average sense. However, it has been shown in [Delluc, Ageorges, Pateyron and Fauchais (2005)] that plasma jet is not stationary. The lattice Boltzmann method (LBM) may account for the transient nature of the plasma jet and its collision process.

Accordingly, how seems the LB approach to be perfectly practical to simulate plasma jets used in thermal spraying processes which conditioned entirely the behaviour of the transported powdery material?

The LBM models are typically built in Cartesian coordinates. Some axisymmetric models allowing 3D economies have been developed recently. The axisymmetric model of Zhou (2008) has been successfully used by Djebali and his co-workers [Djebali, Pateyron, El Ganaoui and Sammouda (2009); Djebali, El Ganaoui, Pateyron and Sammouda (2011)] to simulate argon plasma jet using a large scale turbulence model (Large Eddy Simulation: LES).

In the present study we present the LB simulation results focusing on the high computational aspect showed in predicting the centerline and the transverse development of the plasma jet fields' profiles and also their distributions within the computational domain. We investigate, in addition, the dynamic and thermal behaviours of sprayed alumina particles (Al_2O_3). The results of our model are compared to former measurements and numerical findings for particle diameters ranging from 10 to 100 microns. Throughout this comparison exercise we'll show the agreement level between the different results and then the effectiveness of the LB method to predict the plasma properties which determine absolutely the in-flight particles behaviors, which is the subject of the last part. Finally, concluding remarks are drawn.

2 Numerical modeling

2.1 The lattice Boltzmann background

The lattice Boltzmann Method (LBM) plays actually an alternative tool to the classical macroscopic Navier–Stokes approach solvers in CFD. This new powerful tool

uses mesoscopic technique to simulate fluid flows, heat and mass transfers. In this particle method, the collected informations from movement and interactions of fluid particles are used to simulate the macroscopic fluid behaviour. During the computational process, each iteration is solved based on two coupled steps: the collision (exchange of dynamic, thermal and mass informations between the fluid particles) and the streaming step (movement in discrete directions to adjacent nodes).

In the philosophy of the lattice Boltzmann method, the computational domain is generally discretized in uniform Cartesian cells taking a set number of distribution functions f_k which model the number of fluid particles (9 for the two-dimensional D2Q9 LB model, see Fig. 1), the averaged particles characteristics at each node give the macroscopic quantities such as pressure, velocity, temperature and concentration. The LB approach, itself, is founded on the kinetic gas theory and statistic mechanics and based on the discretization of the kinetic Boltzmann equation. The introduction of the BGK approximation brings a significant simplification of the method by linearization of the complex collision operator around the distribution function in local equilibrium f_k^{eq} . The Boltzmann equation without external forces can be presented as follows:

$$\frac{\partial f}{\partial t} + \vec{c} \cdot \vec{\nabla} f = \frac{1}{\tau} (f^{eq} - f) \quad (1)$$

And the general discrete Boltzmann equation with external forcing term is formulated as:

$$f_k(\vec{x} + \vec{e}_k \Delta t, t + \Delta t) = f_k(\vec{x}, t) + \frac{\Delta t}{\tau_v} (f_k^{eq}(\vec{x}, t) - f_k(\vec{x}, t)) + \Delta t \vec{F}_k \quad (2)$$

where f^{eq} is the equilibrium distribution function, $\Delta \vec{x} = \vec{e}_k \Delta t$, Δt denotes the lattice time step, \vec{F}_k is the external force, τ_v is the lattice relaxation time and \vec{e}_k is the discrete lattice velocity defined in the present D2Q9 model as:

$$\vec{e}_k = \begin{cases} (0, 0), & k = 0 \\ (\cos[(k-1)\pi/2], \sin([(k-1)\pi/2])) c, & 1 \leq k \leq 4 \\ \sqrt{2}(\cos[(2k-9)\pi/4], \sin([(2k-9)\pi/4])) c, & 5 \leq k \leq 8 \end{cases} \quad (3)$$

Where $c = \Delta x / \Delta t$.

The local equilibrium distribution function is formulated according to the problem to be solved, for the D2Q9 model, it is calculated each time step as:

$$f_k^{eq} = w_k \rho \left(1 + \frac{\vec{e}_k \cdot \vec{u}}{c_s^2} + \frac{1}{2} \frac{(\vec{e}_k \cdot \vec{u})^2}{c_s^4} - \frac{1}{2} \frac{\vec{u} \cdot \vec{u}}{c_s^2} \right) \quad (4)$$

where w_k is a weighting factor: $w_0 = 4/9, w_{1-4} = 1/9, w_{5-8} = 1/36, c_s = c/\sqrt{3}$ and ρ is the fluid density.

For non-isothermal flows, we consider a new distribution function g for the temperature field, which its time evolution lattice Boltzmann equation is expressed in the present D2Q4 thermal model as:

$$g_k(\vec{x} + \vec{e}_k \cdot \Delta t, t + \Delta t) = g_k(\vec{x}, t) + \frac{\Delta t}{\tau_\alpha} (g_k^{eq}(\vec{x}, t) - g_k(\vec{x}, t)) \tag{5}$$

The corresponding equilibrium distribution function is defined as:

$$g_k^{eq} = \omega_k T \left(1 + \frac{\vec{c}_k \cdot \vec{u}}{c_s'^2} \right) \tag{6}$$

Where $\omega_{k=1-4} = 1/4$ and $c_s' = c/\sqrt{2}$.

Having computed the local distribution functions values, the flow density, momentum and temperature are defined as:

$$\rho(\vec{x}, t) = \sum_k f_k, \rho \vec{u}(\vec{x}, t) = \sum_k \vec{e}_k f_k \text{ and } T(\vec{x}, t) = \sum_k g_k \tag{7}$$

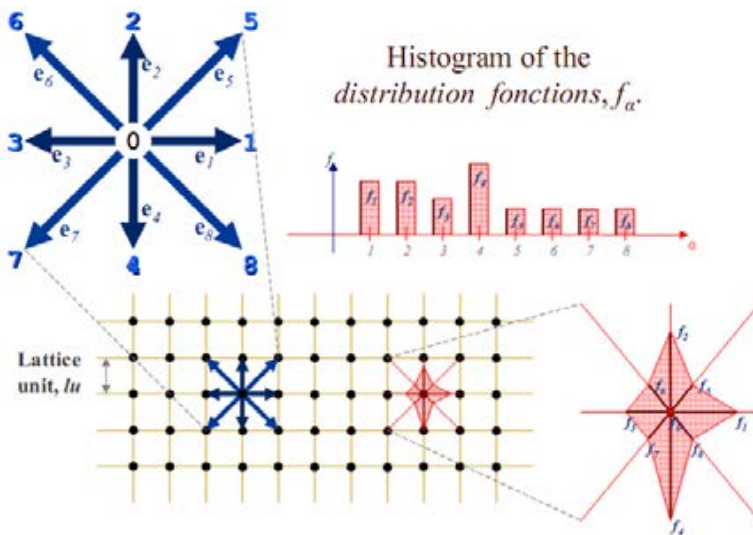


Figure 1: Descriptive elements of the lattice Boltzmann method (LBM) according to [Sukop and Thorne (2006)] in a D2Q9 model.

2.2 Thermal axisymmetric model

The flow governing equations, written under suitable assumptions (see Zhou (2008)) are solved using a D2Q4 scalar formulation of the lattice Boltzmann method for heat field and a D2Q9 formulation for the momentum equation assuming incompressible or compressible flow as in [Pateyron, Elchinger, Delluc and Fauchais (1996)]. The scattering parameters are considered temperature dependent. The discretized equations of the proposed model are given for the mass (f_k) and thermal (g_k) double populations:

$$\begin{cases} f_k(\vec{x} + \Delta\vec{x}, t + \Delta t) - f_k(\vec{x}, t) = -[f_k(\vec{x}, t) - f_k^{eq}(\vec{x}, t)]/\tau_v \\ \quad + \Delta t \cdot F_1 + \Delta t \cdot e_{ki} F_{2i}/6, & k = 0 - 8 \\ g_k(\vec{x} + \Delta\vec{x}, t + \Delta t) - g_k(\vec{x}, t) = -[g_k(\vec{x}, t) - g_k^{eq}(\vec{x}, t)]/\tau_\alpha \\ \quad + \Delta t \cdot S, & k = 1 - 4 \end{cases} \quad (8)$$

Where S , F_1 et F_{2i} are space functions deriving from axisymmetric formulations. The relaxation times τ_v and τ_α are linked to the kinetic viscosity and thermal diffusivity: $\nu = (\tau_v - 0.5)\Delta x^2/3\Delta t$ and $\alpha = (\tau_\alpha - 0.5)\Delta x^2/2\Delta t$, further details can be found in [Djebali (2011)].

The macroscopic variables are calculated using the zeroth and first order moments at each lattice node as in Eq. 7.

2.3 Temperature dependent diffusion parameters

The plasma jet is flowing at high temperatures. Thus, all physical quantities (dynamic viscosity, thermal conductivity...) depend significantly on the temperature (Fig. 2 and Fig. 3). One of the objectives of this study is to extend the use of the LB method by using variable diffusion parameters. In general cases, if LB_{scale} is the lattice Boltzmann scale for a field ϕ and Ph_{scale} is its analogue in the physical space, then the dimensionless quantity is invariant in its transition from lattice Boltzmann space (LB) to physic space (Ph):

$$\phi_{LB}/LB_{scale} = \phi_{Ph}/Ph_{scale} \quad (9)$$

This allows us to draw up a conversion table between the LB and Ph quantities (see Djebali (2011)).

2.4 Turbulence modeling

In LB turbulent flow models, the viscosity is adjusted locally by adding the eddy viscosity to molecular viscosity. For the chosen D2Q9 lattice, the effective viscosity

obeys the following equation:

$$v_{tot} = \frac{\tau_{v-eff} - 0,5}{3} = v + v_t = v + (C_s \Delta)^2 |\bar{S}_{ij}| \tag{10}$$

Intermediate calculations lead to a quadratic equation, which gives:

$$\tau_{v-tot} = \tau_{v-eff}(x, t) = \left(\tau_v + \sqrt{\tau_v^2 + 18 (C_s \Delta)^2 |Q_{ij}| / \rho(x, t)} \right) / 2 \tag{11}$$

Where $Q_{ij} = \sum_k e_{ki} e_{kj} (f_k - f_k^{eq})$ and Δ be the filter width equal to the space unit.

Same for the thermal field, the relaxation time is adjusted using the new thermal diffusivity:

$$\alpha_{tot} = \frac{\tau_{\alpha-eff} - 0,5}{2} = \alpha + \alpha_t = \alpha + \frac{v_t}{Pr_t} \tag{12}$$

Where Pr_t is the turbulent Prandtl number, usually taken between 0.3 and 1.

2.5 In-flight particles model

The equations are expressed as in Djebali (2011):

$$\frac{d\vec{x}_p}{dt} = \vec{u}_p, m_p \frac{d\vec{u}_p}{dt} = \vec{F}_p = C_D \frac{\pi d_p^2}{8} \rho_g |\vec{u}_g - \vec{u}_p| (\vec{u}_g - \vec{u}_p) \tag{13}$$

Where $\vec{x}_p, \vec{u}_p, \vec{F}_p, m_p$ and d_p are respectively the particle position, velocity, drag force, mass and diameter. \vec{u}_g, ρ_g are the local jet velocity and density. C_D is the drag coefficient modified by factors introduced to account for strongly varying plasma properties and to incorporate non-continuum effects in the particles boundary layers [Dyshlovenko, Pateyron, Pawlowski and Murano (2004); Pateyron (website)].

The particle motion and heat-up equations are marched out in the time using a second-order temporal finite differences approximation to the time derivatives. The powder injector diameter $d_{inj}=1.8\text{mm}$ is centred at (5mm,-7mm) in a 2D coordinate system (z, r). Alumina powder is used, the particle is assumed to be spherical and thermally thin (assuming low Biot number, eg $Bi < 0.01$). The thermo-physical properties of alumina (Al_2O_3) powder can be drawn from [Pateyron (website)].

3 Computational domain and inlet profiles

The computational domain is a half-plane of $100\text{mm} \times 12\text{mm}$ (Fig. 4). The nozzle exit is governed by parabolic temperature and velocity profiles, as follows:

$$\begin{cases} u_{in}(r) = U_{max}(1 - (r/R_{in})^2) \\ T_{in}(r) = (T_{max} - T_{min})(1 - (r/R_{in})^4) + T_{min} \end{cases} \tag{14}$$

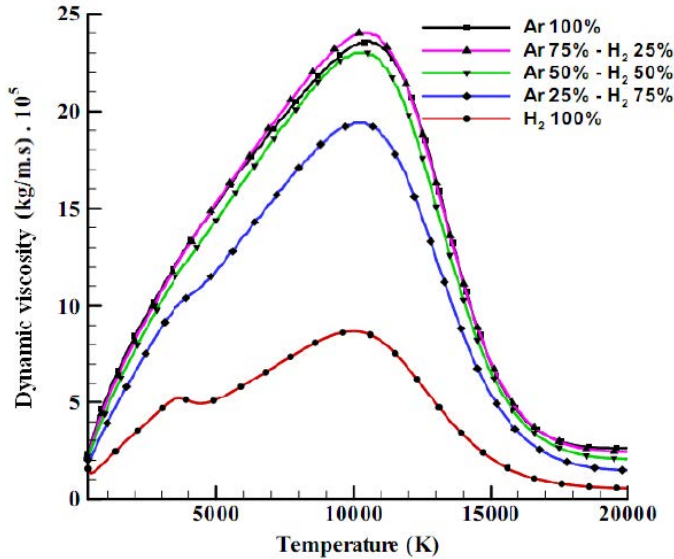


Figure 2: Thermal conductivities of pure gases Ar, N₂ and Ar-N₂ mixtures for different proportions at atmospheric pressure.

More details are given in [Djebali (2011)] on boundary conditions and the operating conditions adopted in *Jets&Poudres* code used for purpose of validation.

4 Results and discussions

In this work we have first drawn a validation analysis based on free jet. Therefore, the boundary CD is considered as a free boundary. The present LB results based on the centerline axial-velocity (Fig. 5) and temperature (Fig. 6) are compared to numerical and experimental results of Pfender and Chang [Pfender and Chang (1998)] and the results of the code *Jets&Poudres* for specified jet conditions.

One can observe that the axial temperature gradient near the inlet region (interval 0-30mm) is close to 220 K/mm then close to 200 K/mm observed experimentally (counter 136 K/mm and 152 K/mm for *Jet & Poudres* and Pfender and Chang results respectively) and the velocity gradient is close to 8.8 (m/s)/mm (counter 10.48 (m/s)/mm and 9.48 (m/s)/mm for *Jet & Poudres* and Pfender and Chang results respectively) which agree well with former experimental and numerical observations. It is also clear that our results go well with *Jet & Poudres* ones. The disparity between the two results in the potential core of the plasma jet (hot zone) is probably due to the fact that ramps are used in *Jet & Poudres* code for the inlet temperature

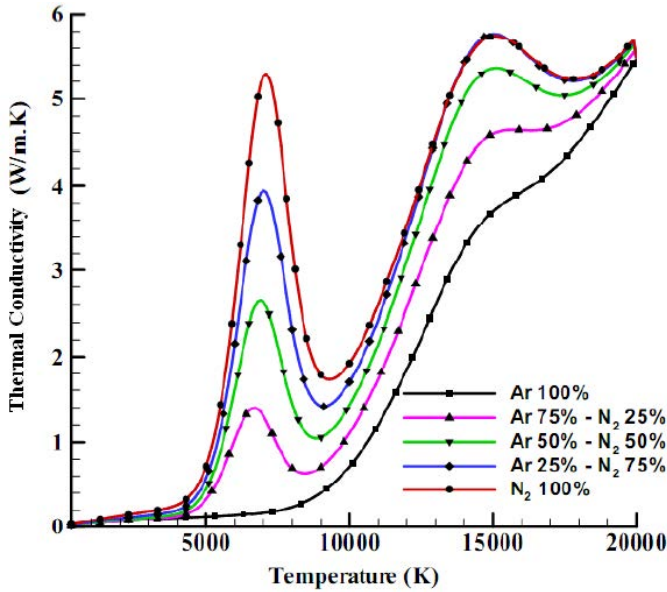


Figure 3: Dynamic viscosities of pure gases Ar, H₂ and Ar-H₂ mixtures for different proportions at atmospheric pressure.

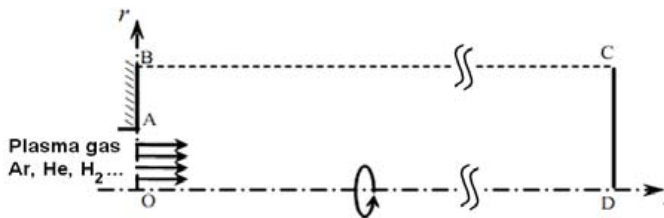


Figure 4: Sketches of the area to be modeled between dotted lines. An axisymmetric jet model is considered here.

and velocity profiles instead of ours parabolic ones. After that, far from the nozzle exit, the profiles become Gaussian and the two curves go together.

Furthermore, the present predictions for the velocity field align well with the *Jets&Poudres* results without significant deviation from experimental results. While for the temperature distribution, our prediction compares very well the Pfender and Chang numerical and experimental results, which gives our results the advantage of being a compromise between the results of different numerical models and experimental findings.

We have investigated, also, the isotherms and iso-axial velocities distributions of our results and those of *Jets&Poudres* (not presented here, see [Djebali (2011)]). We have remarked from LB results that the temperature distribution is more expanded than the axial-velocity one, and it shares this characteristic with the Finite-Difference (*Jet & Poudres*) results; in addition, that *Jets&Poudres* jet is more expanded and that our results are consistent with the most previous predicted results [Xu, Wu and Chen (2003)] where the jet width does not exceed at all 10 mm for the temperature and velocity distributions. This behaviour, for LB results, is in good agreement with experimental plasma-jet characteristics because plasma jet is more extended, however *Jet & Poudres* results are more representative for flame jet which is more expanded.

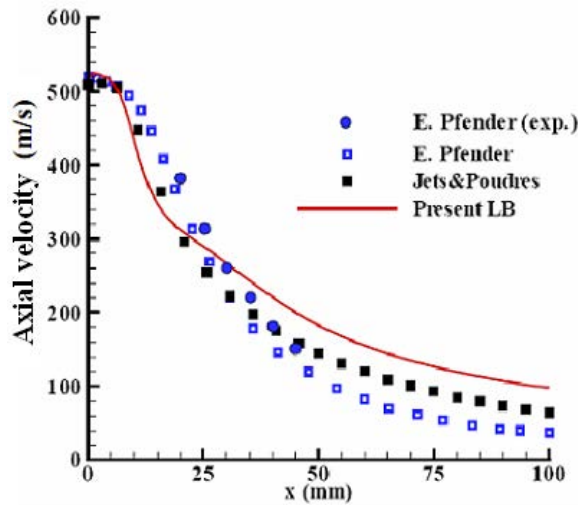


Figure 5: Centerline plasma jet velocity for inlet flat temperature profile compared with previous findings.

Fig. 7 shows the radial distributions of the analytic and the simulated axial velocity and temperature at different sections from the nozzle exit. The Gaussian profiles for the two fields hold for all the cross sections, the present predictions are found to match well the well-known dimensionless form (i.e reduced quantities) of the velocity and temperature fields, these forms are expressed as:

$$\begin{cases} \frac{U(r,z)}{U_c(z)} = \exp[-\ln(2)\eta_U^2] \\ \frac{T(r,z)}{T_c(z)} = \exp[-\ln(2)\eta_\theta^2] \end{cases} \quad (15)$$

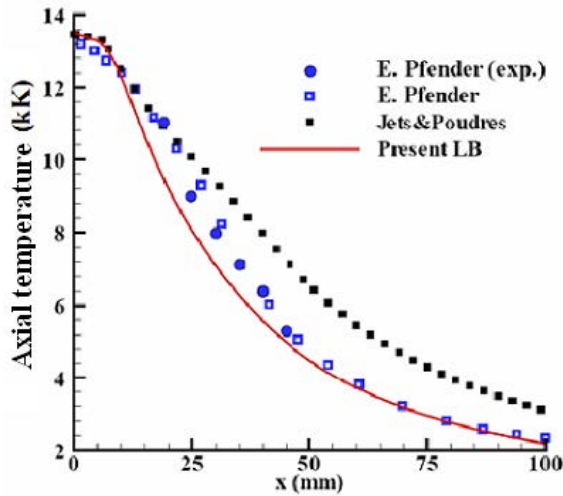


Figure 6: Centerline plasma jet temperature for inlet flat temperature profile compared with previous findings.

Where $\eta_{\phi} \bar{\delta}_{0.5}$ is the transverse distance such as $\phi(r, z)/\phi_c(z) = 0.5$, $\phi_c(z) = \phi(0, z)$ and ϕ plays for U or T .

The second part of this work consists of studying the characteristics of spraying alumina (Al_2O_3) powder. The results of spraying of two alumina particles (separately) sized $25\mu\text{m}$ and $45\mu\text{m}$ at different injection velocities are presented in Fig. 8 (a, b and c). It is clear that the trajectories predicted by the two methods (LB and FD) are in very good agreement, while a little deviation is observed for the axial velocity profiles in the region 0-30mm. This discrepancy is probably due to the use of flat profiles at the torch exit in the code *Jets&Poudres*, so the derived velocities are higher. After this region, the expansion behaviour in a free jet occurs similarly and the two results are similar at the jet exit. This result is coherent with conclusions drawn for the plasma jet fields since their distributions affect directly the particles momentum and heat up.

Fig. 9 (a, b and c) show the effect of particle size dispersion (Gaussian distribution) on the powder trajectory, velocity and temperature profiles. The diameters vary between $15\mu\text{m}$ and $75\mu\text{m}$, the injection velocity is $u_{inj}=10\text{m/s}$. The average profiles ($d_p=45\mu\text{m}$) are also presented. It is clear that the particle size dispersion has a major effect on the particles spraying behaviours; which will influence differently the behaviour during the impact on the target. Then, we can say that through a powder size analysis, we can predict the spray width and consequently enhancing

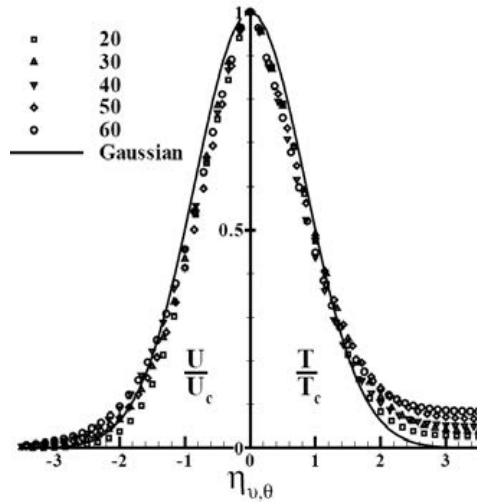


Figure 7: Development of transverse velocity (left) and temperature (right) profiles compared with the centred Gaussian (solid line) for different sections.

the projection efficiency. We can also say that increasing the particle size (at same u_{inj}) leads to a radial exit.

Contrarily, reducing the particle size, the particle will be rejected due to a momentum default. Then, it acquires a slightly high axial velocity near the jet velocity edge (Fig. 9: (b) and (c)), resulting in a particle sub-heating.

In parallel to the size effect on dynamic and thermal behaviors, we have investigated in [Djebali (2011)] the effects of injection velocity, injection position along the injector diameter and injection angle separately, we concluded that major differences are introduced. Finally, we are interested in examining the effect of dispersion of all parameters (size, speed, position and injection angle) simultaneously on the trajectories, velocity profile and temperature fields.

Under the adopted conditions (see Djebali (2011)), the results of our simulation, for $u_{max} = 10\text{m/s}$ (u_{max} is the maximum velocity for a parabolic injection profile), are shown in Fig. 10 (a, b and c). We note that these profiles clearly differ from all the profiles presented above where we study the effect of each parameter separately, which highlights the interaction of dispersions for injection and their effects on the dynamic and thermal behaviours of sprayed powder.

We concluded that for $u_{max} \sim 10\text{m/s}$, the droplets arrive sub-heated. However for $u_{max} \sim 25\text{m/s}$, the arrival parameters (averaged radial position, velocity and temperature) are reasonable $T_{avg} \sim 2200\text{K}$ and $U_{avg} \sim 100\text{m/s}$ (avg means averaged

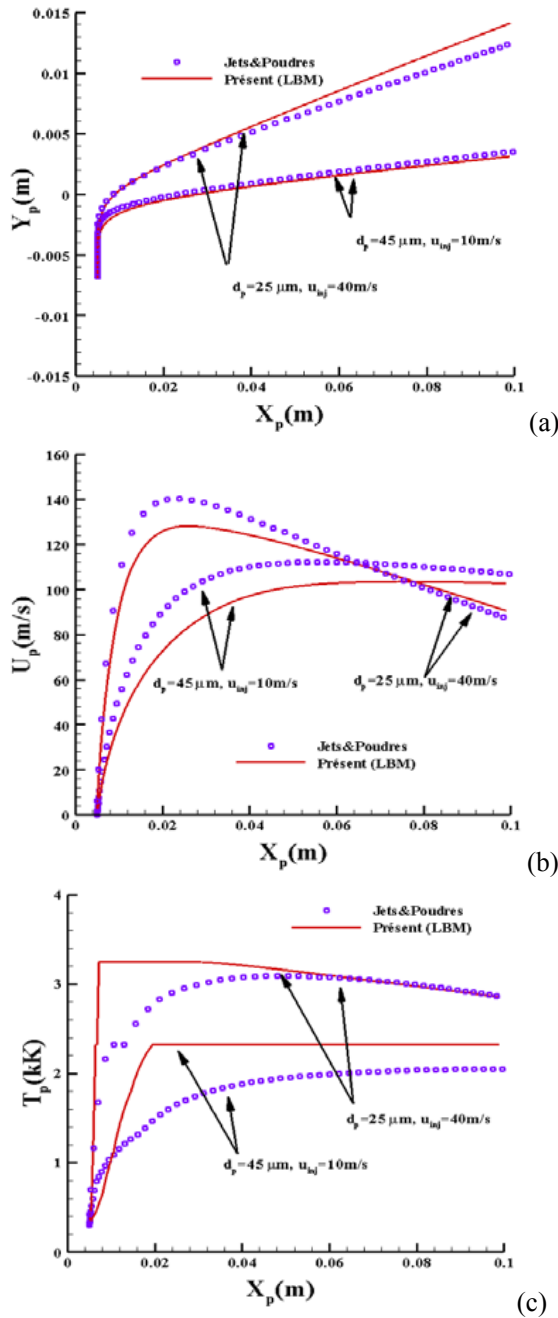
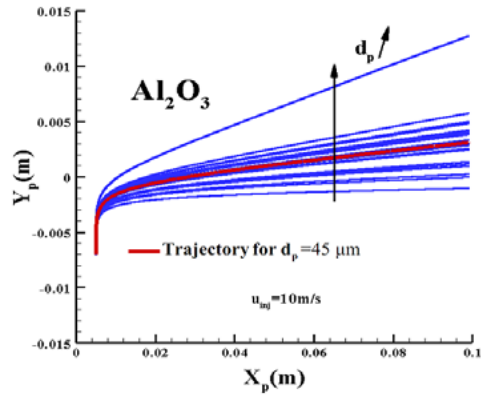
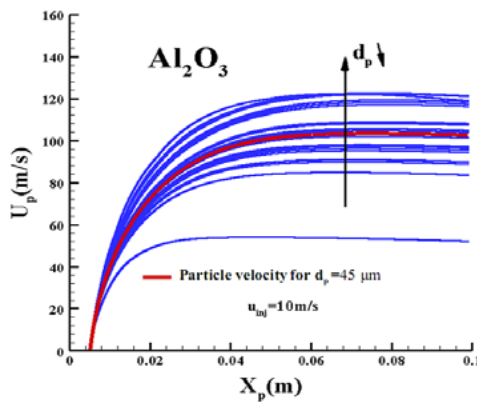


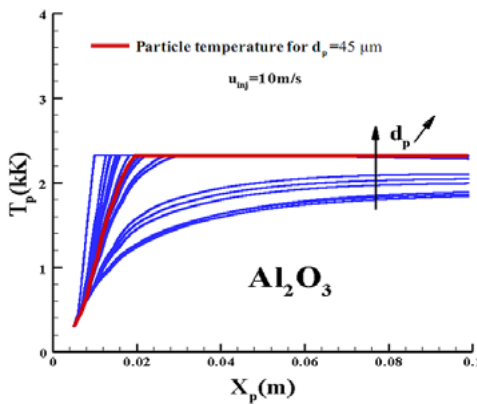
Figure 8: Comparison of trajectories (a), axial velocities (b) and temperatures (c) profiles: our results (LBM) and the results of *Jets&Poudres* for two dense Al_2O_3 particles injected at different injection velocities.



(a)

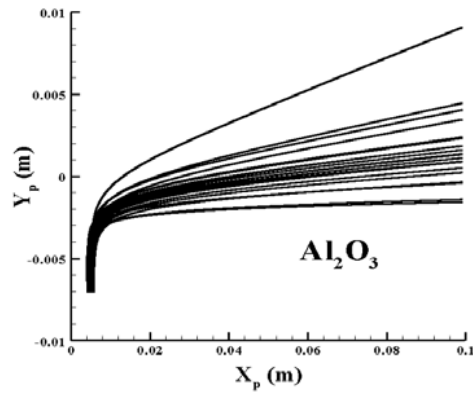


(b)

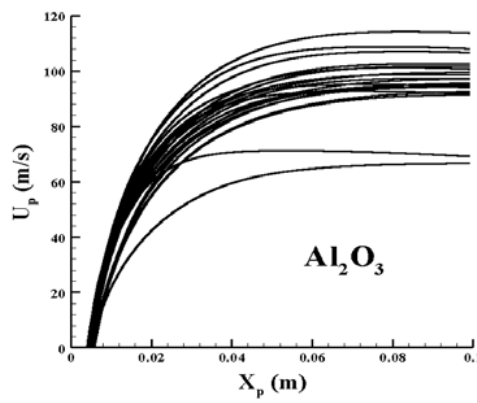


(c)

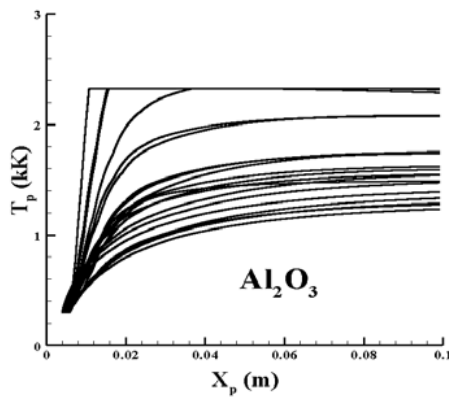
Figure 9: Distributions of trajectories (a), axial velocities (b) and temperatures (c) profiles. A sample of particles is used to investigate the Gaussian dispersion effects in particles diameters: $d_p \sim N(45,10)$. Mean profiles are also presented.



(a)



(b)



(c)

Figure 10: Effects of dispersion at injection point on the distributions of trajectories (a), axial velocities (b) and temperatures (c) profiles for sample of particles.

value).

5 Conclusion

In this paper, we have investigated the dynamic and thermal behaviours of spraying particles. A comparison was drawn on test case of alumina powder of different sizes injected at different velocities, showed that our results are in excellent agreement with the results of the *Jets&Poudres* code. The focus was then put on the effect of injection dispersing for alumina powder on the dynamic and thermal behaviours of particles in-flight. We concluded that the interactions of these parameters result in a more realistic projection field and the arrival parameters at impact with the substrate are quite reasonable. We concluded also on the high efficiency of the lattice Boltzmann approach in simulating complex thermal flows with temperature dependent diffusion parameters.

Acknowledgement: This work was supported in part by the Ministry of Higher Education and Scientific Research of Tunisia.

References

- Arcondéguy, A.; Gasgnier, G.; Montavon, G.; Pateyron, B.; Denoirjean, A.; Grimaud, A.; Huguet, C.** (2007): Flame-sprayed glaze coatings: Effects of operating parameters and feedstock characteristics onto coating Structures. *Journal of Thermal Spray Technology* 16 (5-6), pp. 978-990.
- Ben Ettouil, F.; Mazhorova, O.; Pateyron, B.; Ageorges, H.; El Ganaoui, M.; Fauchais, P.** (2008): Predicting dynamic and thermal histories of agglomerated particles injected within a d.c. plasma jet, *Surface & Coatings Technology*, vol. 202, pp. 4491-4495.
- Brilhac, J.F.; Pateyron, B.; Delluc, G.; Coudert, J.F.; Fauchais, P.** (1995): Study of the dynamic and static behavior of dc vortex plasma torches: Part I: Button type cathode, *Plasma Chem. Plasma Process.* vol. 15, no. 2, pp. 231-255.
- Chen, W.L.T.; Heberlein, J.; Pfender, E.; Pateyron, B.; Delluc, G.; Elchinger, M.F.; Fauchais, P.** (1995): Thermodynamic and transport properties of argon/helium plasmas at atmospheric pressure. *Plasma Chem. Plasma Process.*, vol. 15, no.3, pp. 559-579.
- Delluc, G.; Ageorges, H.; Pateyron, B.; Fauchais, P.** (2005): Fast modelling of plasma jet and particle behaviours in spray conditions. *High Temp. Mat. Processes*, vol. 9, no. 2, pp. 211-226.
- Dilawari, A. H.; Szekely, J.** (1987): Some Perspectives on the modeling of plasma

jets; *Plasma Chem. Plasma Process.*, vol. 7, no. 3, pp. 317-339.

Djebali, R. (2011): *Simulation et modélisation des transferts dans les milieux multiphasés et multiconstituants par une approche Boltzmann sur réseau*. Thèse de doctorat, Univ. Tunis el Manar.

Djebali, R.; El Ganaoui, M.; Pateyron, B.; Sammouda, H. (2011): Simulation and modeling of turbulent plasma jet based on axisymmetric LBGK model. *Defect and diffusion Forum*, vols. 312-315, pp.1167-1171.

Djebali, R.; Pateyron, B.; El Ganaoui, M.; Sammouda, H. (2009): Axisymmetric high temperature jet behaviours based on a lattice Boltzmann computational method. Part I: Argon Plasma. *Int. Rev. Chem. Eng.*, vol. 1, no. 5, pp. 428-438.

Dyshloenko, S.; Pateyron, B.; Pawlowski, L.; Murano, D. (2004): Numerical simulation of hydroxyapatite powder behaviour in plasma jet. *Surface & Coatings Technology*, vol. 179, no.1, pp. 110-117.

Ghelichi, R.; Bagherifard, S.; Pariente, I.F.; Guagliano, M.; Vezzù, S. (2010): Experimental study of shot peening followed by cold spray coating on residual stresses of the treated parts. *SDHM: Structural Durability & Health Monitoring*, vol. 6, no. 1, pp. 17-30.

Li, D.; Saheli, G. ; Khaleel, M. ; Garmestani H. (2006): Microstructure optimization in fuel cell electrodes using materials design. *CMC: Computers, Materials, & Continua*, vol. 4, no. 1, pp. 31-42.

Pateyron, B. (1987): Thèse de doctorat d'État Université de Limoges. No 21-1987.

Pateyron, B.: 'Jets&Poudres' free download from: <http://www.unilim.fr/spcts> or <http://jets.poudres.free.fr>

Pateyron, B.; Elchinger, M.F.; Delluc, G.; Fauchais, P. (1996): Sound velocity in different reacting thermal plasma coatings *Plasma Chem. Plasma Process.*, vol. 16, no. 1, pp. 39-57.

Pfender, E.; Chang, C. H. (1998): Plasma spray jets and plasma-particulates interactions: modeling and experiments. *Proceeding of the 15th International thermal spray conference*. 25-29 May 1998, Nice, France.

Siagam, A.T.; Brenner, G.; Giese, P. ; Wesling V. (2008): Numerical and experimental study of particle motion in plasma arc welding. *FDMP: Fluid Dynamics & Materials Processing*, vol. 4, no. 2, pp. 77-84.

Sukop, M.C.; Thorne, D.T. (2006): *Lattice Boltzmann modeling: an introduction for geoscientists and engineers*. Springer, Berlin.

Xie, H.; Koshizuka, S.; Oka, Y. (2007): Modeling the wetting effects in droplet impingement using Particle Method. *CMES: Computer Modeling in Engineering & Sciences*. vol. 18, no. 1, pp. 1-16.

Xu, D.Y.; Wu, X.C.; Chen, X. (2003): Motion and heating of non-spherical particles in a plasma jet. *Surface & Coatings Technology*, vol. 171, no.1-3, pp. 149-156.

Zhou, J. G. (2008): Axisymmetric lattice Boltzmann method. *Physical Review E*, vol. 78, no. 3, 036701.

